Dyes and Pigments 112 (2015) 138–144

Contents lists available at ScienceDirect

Dyes and Pigments

journal homepage: www.elsevier.com/locate/dyepig

Influence of bulky pyrrolyl substitent on the physicochemical properties of porphyrazines

Tomasz Koczorowski [a], Wojciech Szczolko [a], Kvetoslava Burda [b], Magdalena Nowak [a], Malgorzata Dawidowska [a], Anna Teubert [c], Lukasz Sobotta [d], Maria Gdaniec [e], Jozef Korecki [b], Jadwiga Mielcarek [d], Ewa Tykarska [a, *], Tomasz Goslinski [a, *]

[a] Department of Chemical Technology of Drugs, Poznan University of Medical Sciences, Grunwaldzka 6, 60-780 Poznan, Poland
[b] AGH University of Science and Technology in Krakow, Faculty of Physics and Applied Computer Science, Al. Mickiewicza 30, 30-059 Krakow, Poland
[c] Institute of Bioorganic Chemistry, Polish Academy of Sciences, Z. Noskowskiego 12, 61-704 Poznan, Poland
[d] Department of Inorganic and Analytical Chemistry, Poznan University of Medical Sciences, Grunwaldzka 6, 60-780 Poznan, Poland
[e] Faculty of Chemistry, Adam Mickiewicz University, Umultowska 89b, 61-614 Poznan, Poland

ARTICLE INFO

Article history:
Received 16 April 2014
Received in revised form
25 June 2014
Accepted 27 June 2014
Available online 7 July 2014

Keywords:
Macrocyclization
Porphyrazine
Crystal structure
Mössbauer spectroscopy
Iron valence and spin states
Dimers

ABSTRACT

The synthesis and characterization of porphyrazines possessing 2,5–diphenylpyrrol-1-yl and dimethylamino peripheral groups and their precursors are shown. Bulky pyrrolyl substituents influenced the physicochemical properties and solid-state structure of novel porphyrazines and did not hamper the formation of the porphyrazine associates in solution and solid-state. Occurrence of centrosymmetric dimers in single crystal X-ray structure of magnesium(II) porphyrazine with Mg···Mg distance of ca. 11.2 Å, impacted by interdigitation of the phenyl substituents, was noticed. In addition, an iron(II) porphyrazine derivative was investigated. The importance of Mössbauer spectroscopy in the assessment of valence and spin state of the iron ion inside the core of the iron(II) porphyrazine is shown.

1. Introduction

Porphyrazine (Pz) macrocycles, due to their special photochemical and electrochemical properties, have proved their potential for diverse medical (photosensitizers) and technological applications (catalysts, sensors). Pzs can be modified by the exchange of the metal cation inside the core or by peripheral modifications in their β positions with aliphatic, aryl, sulfur, oxygen and nitrogen residues [1–5]. Some Pzs have demonstrated a strong affinity towards metal ions, including $Fe^{2+/3+}$ [5,6]. Iron Pzs have been considered a potential catalyst in oxidation reactions [7,8]. Although, Pzs possessing β,β-substituted, fused, heterocyclic rings have been widely studied [9,10], there has been only limited data on those modified by peripheral 5-membered ring heteroaromatic group attachment. One of the examples is a two-core Pz reported by Luo et al. [11], that is substituted with trimethyl-3-thienyl groups on its periphery. The other Pzs bearing peripheral 2,5-dimethylpyrrol-1-yl, and 2,5-dithienylpyrrol-1-yl originate from our group [12–15]. Below we describe the synthesis of novel hybrid molecules that have properties beyond the sum of the Pz macrocycles and 2,5–diphenylpyrrol-1-yl fragments. These include the formation of centrosymmetric dimeric associates of magnesium(II) Pz molecules by interdigitation of their bulky substituents, as observed in the crystal. Bulky pyrrolyl substituents on the periphery of iron(II) Pz influence its physicochemical properties, which was confirmed by Mössbauer spectroscopy.

2. Experimental section

2.1. General procedures

All reactions were conducted in oven dried glassware under argon. All solvents were rotary evaporated at or below 50 °C. Reaction temperatures reported refer to external bath temperatures. Methanol, tetrahydrofurane and dichloromethane were distilled. Other solvents and all reagents were obtained from commercial suppliers and used without further purification unless otherwise stated. Melting points were obtained on a “Stuart” Bibby apparatus

* Corresponding authors. Tel.: +48 61 854 66 31.
E-mail addresses: etykarsk@ump.edu.pl (E. Tykarska), tomasz.goslinski@ump.edu.pl (T. Goslinski).

http://dx.doi.org/10.1016/j.dyepig.2014.06.033
0143-7208/

and are uncorrected. Dry flash column chromatography was carried out on Merck silica gel 60, particle size 40–63 μm. Thin layer chromatography (TLC) was performed on silica gel Merck Kieselgel 60 F_{254} plates and visualized with UV (λ_{max} 254 or 365 nm). UV–Vis spectra were recorded on a Hitachi UV–Vis U-1900 spectrometer; λ_{max} (logε), nm. Elemental analysis and mass spectra (ES, MALDI TOF) were carried out by the Advanced Chemical Equipment and Instrumentation Facility at the Faculty of Chemistry, Adam Mickiewicz University in Poznan. HRMS (ESI) spectra were detected on a Thermo QExactive with the ESI source at the European Center of Bioinformatics and Genomics in Poznan.

2.2. Single crystal X-ray structure determination

Single, prism like yellow crystals of maleonitrile **3** and dark blue plates of magnesium porphyrazine **4a** were grown at room temperature by slow evaporation method from CH_2Cl_2/*n*-hexane (1:1) and EtOH/$CHCl_3$/*n*-PrOH (1:1:0.1) solutions, respectively. The diffraction intensity data were collected with an Oxford Diffraction Xcalibur Eos diffractometer using graphite-monochromated MoKα radiation. The structures were processed with the CrysAlis Pro software [16], solved by direct methods with SIR2004 [17], and refined by full matrix least-squares based on F^2 by SHELXL-97 [18] program. The hydrogen atoms attached to the C atoms were located at geometrically calculated positions and refined in the riding mode with isotropic temperature factors fixed at 1.2(Ueq) of the parent atoms (1.5 for methyl groups). Non-hydrogen atoms in **3** were refined anisotropically, except for the five atoms of the disordered benzene ring having minor occupancy of ca. 12% (Fig. S1, Supplementary data). Crystals of **4a** were poorly diffracting and the number of observed reflections did not allow for anisotropic refinement of non-hydrogen atoms. The highest peaks on the difference-Fourier map in the disordered part of the crystal were identified as propanol and two water solvent molecules and included in the final refinement with partial occupancy. The hydrogen atoms of the propanol O–H groups were located in electron density difference maps and their O–H distances standardized to 0.84 Å. In the final refinement cycles O–H group hydrogen atoms were treated as riding on their parent atoms with Uiso(H) = 1.2 Ueq(O). In case of water molecules, hydrogen-atom positions were not determined. A summary of the structure determination of **3** (CCDC 986312) and **4a** (CCDC 986311) is given in Supplementary data. The asymmetric unit and atom labeling scheme for **3** are shown in Figures S1, S2 (Supplementary data), and for **4a** – in Fig. S3 (Supplementary data).

2.3. NMR studies

^{1}H NMR, ^{13}C NMR spectra were recorded using a Bruker 400 and 500 spectrometers. Chemical shifts (δ) are quoted in parts per million (ppm) and are referred to a residual solvent peak. Coupling constants (J) are quoted in Hertz (Hz). The abbreviations s, d, h, t, and m refer to singlet, doublet, hidden, triplet, and multiplet, respectively. Chemical shifts of aggregated species of Pz **6** are signed with asterisk (*). Additional techniques (^{1}H–^{1}H COSY, HSQC, HMBC) and temperature spectra were used to assist allocation.

2.4. Mössbauer spectroscopy studies

Powder sample frozen to the temperature of liquid nitrogen was placed in a home-built cryostat at 85 K. The temperature was stabilized within 0.03 K. Mössbauer ^{57}Fe spectra were recorded using ^{57}Co(Rh)-50 mCi as a source of 14.4 keV radiation. Hyperfine parameters characterizing valence and spin states of the heme-iron in the investigated Pzs were obtained from the theoretical analysis of experimental spectra by use of Recoil software [19]. Values of isomer shifts are given relative to α-Fe at 295 K.

2.5. Synthetic procedures of 2–6

2.5.1. 2-Amino-3-(2,5-diphenyl-1H-pyrrolyl)-(2Z)-butene-1,4-dinitrile (**2**)

A known compound 2 was synthesized by modifying Begland's procedure [20]: The suspension of DAMN (462 mg, 4.28 mmol) (**1**), 1,2-dibenzoylethane (1.02 g, 4.82 mmol), catalytic amount of TFA (200 μL) and methanol (50 mL) was mixed under reflux for 24 h. After cooling to room temperature, the solvent was evaporated using a rotavapory vacuum evaporator to dryness and purified by column chromatography (CH_2Cl_2) to give small yellow crystals of the desired compound (1.07 g, 80% yield).

2.5.2. 2-Dimethylamino-3-(2,5-diphenyl-1H-pyrrolyl)-(2Z)-butene-1,4-dinitrile (**3**)

Sodium hydride (60% dispersion in mineral oil; 45 mg, 1.13 mmol) was suspended in THF (10 mL) at (−17 °C). Next 2-amino-3-(2,5-diphenyl-*1H*-pyrrolyl)-(2Z)-butene-1,4-dinitrile (**2**) (160 mg, 0.52 mmol) in THF (2 mL) was added and stirred 30 min at temperature (−15 °C). After that $(CH_3O)_2SO_2$ (99 μL, 1.04 mmol) was added dropwise to the reaction mixture for 30 min at (−10 °C) and stirred at room temperature for 20 h. The reaction was carefully quenched by adding water (2 mL) and the reaction mixture was poured into ice-water mixture (100 mL). The resulting yellow precipitate was isolated by filtration to give **3** (160 mg, 91% yield). The crude material was crystalized (CH_2Cl_2-*n*-hexane) to give light yellow crystals: mp 105–107 °C. R_f (CH_2Cl_2) 0.65. UV–Vis (CH_2Cl_2): λ_{max}, nm (logε) 300 (4.39). ^{1}H NMR (400 MHz; $CDCl_3$): δ_H, ppm 2.49 (s, 6H, $N(CH_3)_2$), 6.41 (s, 2H, pyrrole-H), 7.38 (t, ^3J = 8 Hz, 2H, C_6H_5), 7.46 (t, ^3J = 8 Hz, 4H, C_6H_5), 7.52–7.55 (m, 4H, C_6H_5). ^{13}C NMR (100 MHz, $CDCl_3$): δ_C, ppm 41.00 ($N(CH_3)_2$), 91.79, 111.05, 112.19, 118.61, 128.10, 128.42, 128.92, 131.91, 138.75. MS (ES neg): *m/z* 323 $[M-CH_3]^-$. MS (ES pos) 339 $[M+H]^+$, 361 $[M+Na]^+$, 378 $[M+K]^+$. Anal. Calc. for $C_{22}H_{18}N_4$: C, 78.08%; H, 5.36%; N, 16.56%. Found: C, 78.04%; H, 5.44%; N, 16.73%.

2.5.3. [2,7,12,17-Tetrakis(dimethylamino)-3,8,13,18-tetrakis(2,5-diphenyl-1H-pyrrolyl)-porphyrazinato]magnesium(II) (**4a**) and [2,7,12,18-tetrakis(dimethylamino)-3,8,13,17-tetrakis(2,5-diphenyl-1H-pyrrolyl)porphyrazinato]magnesium(II) (**4b**)

Mg turnings (53 mg, 2.16 mmol), a crystal of I_2, and 1-butanol (25 mL) were heated under reflux for 6 h. After the mixture was cooled to room temperature, maleonitrile derivative **3** (491 mg, 1.44 mmol) was added to the reaction mixture and heated under reflux for 20 h. After cooling to room temperature, the dark green mixture was filtered through Celite and evaporated. Chromatography (CH_2Cl_2:CH_3OH, 50:1; *n*-hexane:EtOAc, 7:3; *n*-hexane:CH_2Cl_2:CH_3OH, 7:1:1) was performed to give two products: **4a** (90 mg, 18% yield) as a dark green solid: mp > 300 °C. R_f (*n*-hexane:EtOAc 7:5) 0.83, UV–Vis (CH_2Cl_2): λ_{max}, nm (logε) 302 (3.74), 730 (3.48), 817 (2.96). ^{1}H NMR (400 MHz; pyridine-d_5): δ_H, ppm 3.26 (s, 24H, $N(CH_3)_2$), 6.73 (t, ^3J = 8 Hz, 16H, C_6H_5), 6.92 (t, ^3J = 8 Hz, 8H, C_6H_5), 7.01 (s, 8H, pyrrole-H), 7.48 (dd, ^3J = 8 Hz, ^4J = 1 Hz, 16H, C_6H_5); ^{13}C NMR (100 MHz; pyridine-d_5): δ_C, ppm 42.67 ($N(CH_3)_2$), 110.46, 113.59, 126.68, 128.50, 128.50, 135.11, 140.03, 140.03, 150.35 h, 154.70. MS (MALDI TOF): *m/z* 1378 $[M+H]^+$. HRMS (ESI) Found: $[M+H]^+$ 1377.6078 $C_{88}H_{73}N_{16}Mg$ requires $[M+H]^+$ 1377.6054. **4b** (4 mg, 0.8% yield): mp > 300 °C. R_f (*n*-hexane:EtOAc 7:5) 0.83, (CH_2Cl_2:CH_3OH 50:1) 0.11. UV–Vis (CH_2Cl_2): λ_{max}, nm (logε) 292 (3.98), 342 (3.56), 522 (2.76), 691 (3.49). ^{1}H NMR (400 MHz; pyridine-d_5): δ_H, ppm 3.06 (s), 3.26 (s), 3.30 (s), 3.34 (s), 6.62–6.68 (m), 6.68–6.75 (m), 6.76–6.83 (m), 6.86 (s), 6.90–6.94

(m), 6.98 (s), 7.05 (s), 7.30 (d, $^3J = 8$ Hz) 7.38 (d, $^3J = 8$ Hz), 7.42 (d, $^3J = 8$ Hz), 7.53 (d, $^3J = 8$ Hz). MS (MALDI TOF): *m/z* 1378 $[M + H]^+$. HRMS (ESI) Found: $[M + H]^+$ 1377.6063 $C_{88}H_{73}N_{16}Mg$ requires $[M + H]^+$ 1377.6054.

2.5.4. 2,7,12,17-Tetrakis(dimethylamino)-3,8,13,18-tetrakis(2,5-diphenyl-1H-pyrrol-1-yl)porphyrazine (**5**)

Maleonitrile **3** (338 mg, 1.0 mmol) was heated in dimethylaminoethanol (4 mL) under reflux for 24 h. After cooling to room temperature, the green-violet mixture was evaporated with toluene (2 × 50 mL) to dryness and subjected to column chromatography (*n*-hexane:CH_2Cl_2, 1:2) to give **5** (80 mg, 23% yield) as a dark green solid: mp > 300 °C, R_f (*n*-hexane:CH_2Cl_2, 1:2) 0.77. UV–Vis (CH_2Cl_2): λ_{max}, nm (logε) 302 (4.76), 435 (4.01), 734 (4.32), 791 (4.38). ^{1}H NMR (500 MHz; pyridine-d_5): δ_H, ppm −0.51 (s, 2H, NH), 3.35 (s, 24H, $N(CH_3)_2$), 6.95 (m, 16H, C_6H_5), 6.96 (d, $^3J = 9$ Hz 8H, C_6H_5), 7.00 (s, 8H, pyrrole-H), 7.54–7.56 (m, 16H, C_6H_5). ^{13}C NMR (125 MHz; pyridine-d_5): δ_C, ppm 42.83 ($N(CH_3)_2$), 110.91, 112.01, 125.39, 127.09, 128.55, 128.89, 129.57, 134.91, 140.13, 148.76. MS (MALDI TOF): *m/z* 1356 $[M+H]^+$. HRMS (ESI) Found: $[M + H]^+$ 1355.6358 $C_{88}H_{75}N_{16}$ requires $[M + H]^+$ 1355.6361.

2.5.5. [2,7,12,17-Tetrakis(dimethylamino)-3,8,13,18-tetrakis-(2,5-diphenyl-1H-pyrrolyl)porphyrazinato]iron(II) (**6**)

Porphyrazine **5** (85 mg, 0.063 mmol), $FeBr_2$ (135 mg, 0.63 mmol), 2,6-lutidine (2 mL) were heated in toluene-THF mixture (1:1, 10 mL) under reflux for 20 h. After cooling to room temperature, the green mixture was evaporated to dryness. The dark green solid dissolved in dichloromethane (10 mL) was mixed with aqueous 1 M HCl (10 mL) for 30 min as two-phase system. After that time, the organic layer was mixed with brine (10 mL) for 30 min as two-phase system. The organic layer was separated, dried with anh. $MgSO_4$ and rotavapory evaporated. The residual iron species were removed by extraction in dichloromethane (10 mL) – saturated citric acid solution (10 mL). The dry residue was extensively purified by column chromatography (CH_2Cl_2:CH_3OH, 50:1) to give the porphyrazine **6** as a dark green solid (20 mg, 22% yield): mp > 300 °C. R_f (CH_2Cl_2:CH_3OH, 50:1) 0.17. UV–Vis (CH_2Cl_2): λ_{max}, nm (logε) 296 (4.58), 381 (3.91), 440 (3.90), 691 (3.90), 911 (3.56). ^{1}H NMR (400 MHz; pyridine-d_5): δ_H, ppm 2.69 (s, 24H, $N(CH_3)_2$), 2.91*-3.20* (m, 24H, $N(CH_3)_2$), 6.58 (s, 8H, pyrrole-H), 6.74* (t, $^3J = 6$ Hz, 24H, C_6H_5), 7.00* (s, 8H, pyrrole-H), 7.30 (t, $^3J = 6$ Hz 24H, C_6H_5), 7.50* (d, $^3J = 3$ Hz, 16H, C_6H_5), 7.67 (d, $^3J = 3$ Hz, 16H, C_6H_5). ^{13}C NMR (175 MHz; pyridine-d_5): δ_C, ppm 39.98 ($N(CH_3)_2$), (42.26*-42.63*) ($N(CH_3)_2$), (110.54*), 111.73, 111.73, (128.20*), 128.44, 128.44, (128.44*), 128.82, 134.17, (134.17*), 135.20, 140.37, 140.37, (140.37*), 145.25. MS (MALDI TOF): *m/z* 1409 $[M+H]^+$. HRMS (ESI) Found: $[M + H]^+$ 1409.5503 $C_{88}H_{73}N_{16}Fe$ requires $[M + H]^+$ 1409.5553.

3. Results and discussion

Maleonitrile derivative **3** was obtained in a two-step procedure starting from diaminomaleonitrile (**1**) using the conditions reported by Begland et al. [20] and Baum et al. [21]. Novel maleonitrile **3** was used in the Linstead macrocyclization with magnesium *n*-butanolate in n-butanol to give porphyrazine **4a** possessing an alternate system of peripheral substituents (D_{4h} isomer) as the main product in 18% overall yield (Scheme 1) [5,22]. Interestingly, only a tiny amount (0.8% of the overall yield) of the side-product **4b**, Pz possessing non-alternate system of peripheral substituents (C_s isomer), was obtained. The macrocyclization of **3** in dimethylaminoethanol (DMAE) led to the free base Pz **5** in 23% of the yield [23], that was subsequently metalated, following the literature procedure [24], in toluene-THF-2,6-lutidine mixture with $FeBr_2$ to give Pz **6** in 22% yield (Scheme 1). Noteworthy, the reaction mixture was subjected to a two-step purification procedure consisting of extractions in dichloromethane - aqueous 1 M hydrochloric acid, then brine, and dichloromethane – aqueous saturated citric acid.

All porphyrazines were carefully purified by column chromatography and further analyzed by HPLC. HPLC chromatograms of **4a** showed four separate signals, which, when analyzed by Diode Array Detector (DAD), revealed the same absorption profiles. This occurrence might be explained by association type interaction of porphyrazines in solution leading to the formation of Pz aggregates of diverse size and thus, with different retention time. This was

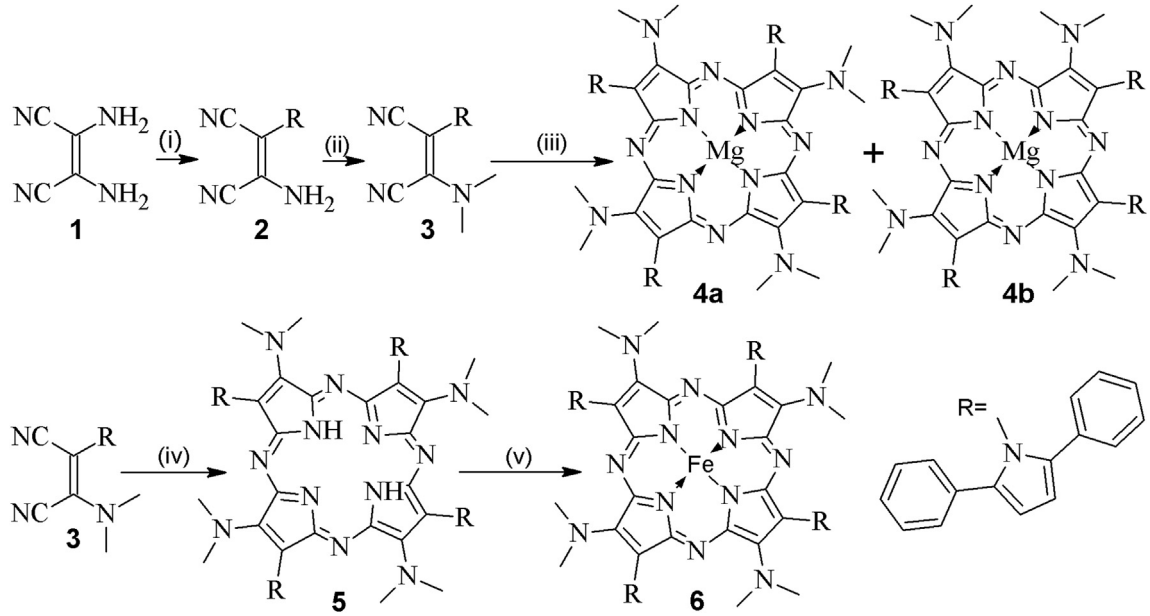

Scheme 1. Reagents and conditions: (i) 1,2-dibenzoylethane, methanol, TFA, reflux, 24 h; (ii) NaH (60% suspension in mineral oil), $(CH_3O)_2SO_2$, THF, −15 °C to rt, 24 h; (iii) Mg(*n*-BuO)$_2$, *n*-BuOH, reflux, 20 h; (iv) DMAE, reflux, 24 h; (v) $FeBr_2$, toluene, THF, 2,6-lutidine, reflux, 24 h; TFA – trifluoroacetic acid.

confirmed by the HPLC analysis of a **4a** sample in the presence of pyridine, which is known to coordinate central metal ions apically (and in this way separates molecules) as only one signal was registered (see Supplementary data). Noteworthy, no aggregation was observed by HPLC for **4b**, **5** and **6**.

All compounds were characterized by UV–Vis, MS and various NMR techniques. Additionally, maleonitrile **3** and Pz **4a** were crystallized to provide single crystals suitable for X-ray structure analyses. The crystal structure of **4a** consists of the [Pz-Mg-propanol] complex (Fig. 1) and disordered solvent molecules. The Mg^{2+} ion is in a square-pyramidal coordination environment with four macrocycle N atoms in the basal plane and 1-propanol O atom in the apical position. The Mg^{2+} cation is displaced from the best plane of four pyrrolyl nitrogens of Pz core toward the O atom by 0.538(3) Å. The orientation of peripheral substituents at pyrrole β,β positions is similar in all porphyrazine subunits. The twist of the $N(CH_3)_2$ groups relative to the macrocycle plane is much smaller [25.9(2) – 40.9(2)°] than of the pyrrole rings of 2,5-diphenylpyrrole fragments [72.4(1) - 80.4(2)°]. The benzene rings from the bulky substituents are protruding on both sides of the macrocycle surrounding the Pz core. In the crystal, the [Pz-Mg-propanol] molecules are assembled into centrosymmetric dimers by interdigitation of the phenyl substituents. These are placed on the Pz side that is free of the auxiliary *n*-propanol ligand (Fig. 1). In the discussed dimer, the Mg···Mg distance of 11.2 Å is larger than found in the other Pzs dimers reported in previous research [5].

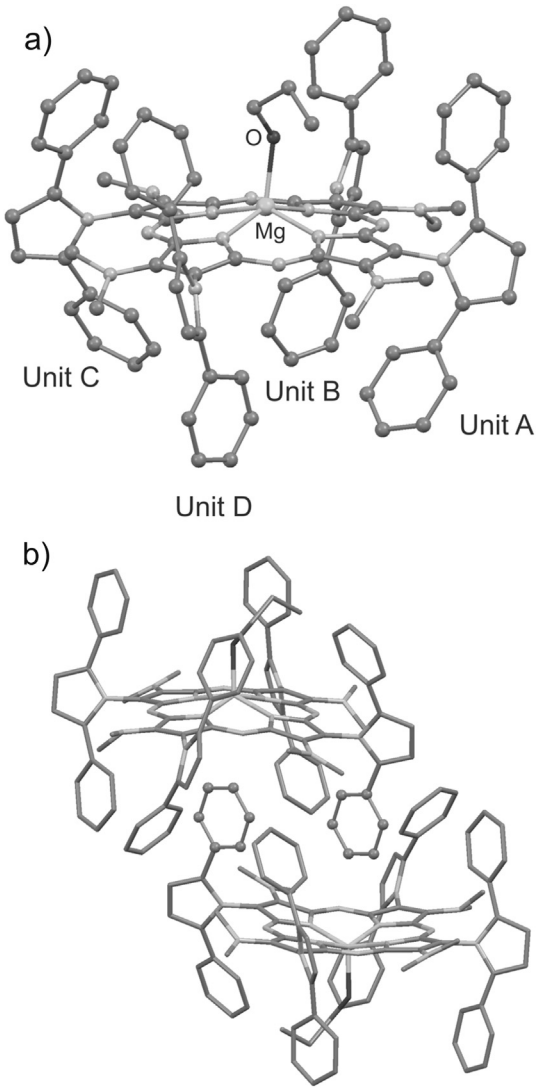

Fig. 1. (a) Molecular structure of Pz **4a** showing the orientation of pyrrole β,β-substituents. Hydrogen atoms are omitted for clarity. (b) Centrosymmetric dimeric associate formed by interdigitated complex molecules in **4a**. Atoms of the encapsulated phenyl ring of unit D are indicated as spheres of arbitrary radii.

Macrocycles **4a**, **5** and **6** were characterized using one and two-dimensional NMR techniques (HMBC, HSQC, COSY) and temperature studies (see Supplementary data). In Pzs COSY spectra, strong cross-peaks between protons of phenyl substituents were observed. Moreover, there appeared in magnesium and free base NMRs explicit couplings between protons belonging to phenyl and pyrrolyl substituents (Fig. 2). The ^{1}H NMR spectra of **6** revealed the presence of two forms of iron Pz: a free, non-aggregated (Pz **6**) and an aggregated (Pz **6***). Such a phenomenon was observed in earlier studies on magnesium and zinc phthalocyanine derivatives [25–27]. It was confirmed in the ^{1}H NMR of **6**, where a single signal of dimethylamino substituents stands for a free form, while divided into multiple signals indicates the formation of associated species. The relative intensity of dimethylamino substituent proton signals of both forms constitutes the ratio of 2:3. In the ^{1}H NMR temperature studies within the range of 273 K–363 K simplifying of multiplied proton signals of the dimethylamino group was observed. Moreover, the ^{1}H NMR measurements recorded after a D_2O addition enabled the determination of the presence of water, coordinated to a Fe^{2+} ion in the core. After the addition of D_2O, the amount of non-coordinated water (water in pyridine-d_5) increased at the expense of the coordinated water.

The absorption spectrum of **4a** has a structure typical of porphyrazines and consists of two intense sharp bands: the Soret band, at 302 nm, and the Q band at 730 nm (Fig. 3). The Q-band transition of **4b** is broad and complex, which is in accordance to the data previously obtained for asymmetrical Pzs with peripheral 2,5-di(2-thienyl)pyrrolyl groups that break the molecular C_4 symmetry [15]. The split and broad Q-band of **5** in dichloromethane is a result of the reduced symmetry of the macrocycle, in accordance with Gouterman's four-orbital model. Pz complex **6** containing Fe^{2+} cation with vacancies on the dπ and/or d_{z2} orbitals showed the expected absorptions in the Soret and Q-band regions. The blue-shifted Soret below 300 nm, the extra Soret band transitions at 381, 440 nm, and the single Q-band at 691 nm with additional absorbance maxima over 900 nm presented in **6** may be due to additional interactions [5,28,29]. It is correlated with a strong affinity to a Fe^{2+} cation to bind different moieties as a result of its electron-acceptor property. Another characteristic that has an influence on the coordination abilities of iron is the structure of the porphyrazine macrocycle ring. An iron Pzs central metal cation is placed outside of a macrocycle plane due to the smaller ring size. This is a consequence of meso-N-bridges in the Pz ring in comparison to meso-C-bridges in porphyrins [7]. Moreover, there is no split in the Q band of **6** (observed in presence of a Fe^{3+} species), which may indirectly suggest the presence of a Fe^{2+} species [30].

The absorption spectra of **4a**, **5** and **6** dissolved at different concentrations in pyridine or dichloromethane were used for aggregation behavior studies. The correlations between the absorbance of the Q-band maximum and the concentrations of the macrocyclic compounds were evaluated. Although these correlations were linear for all compounds, the statistical analysis revealed that the Beer–Lambert law was obeyed only for **6** in both solvents. These data indicate that **5**, unlike **4a**, aggregates in both pyridine and dichloromethane (Figures S4–S9, Table S8 in the Supplementary data). Furthermore, the corresponding spectra of fluorescence excitation and absorption spectra of **4a** support its aggregation behavior study, as they match each other in pyridine, unlike dichloromethane (Figures S10 and S11 in the Supplementary data).

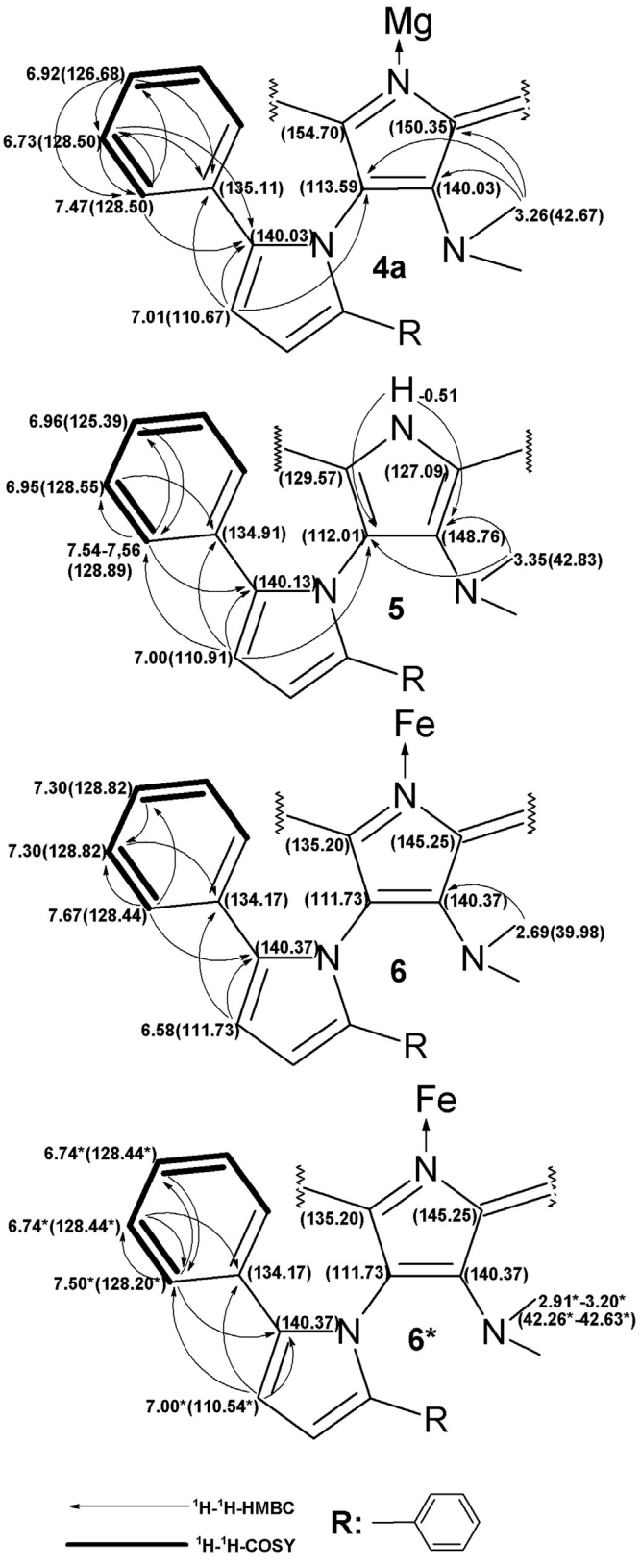

Fig. 2. NMR $^{1}H-^{13}C$ HSQC, $^{1}H-^{13}C$-HMBC and $^{1}H-^{1}H$–COSY connectivities of **4a**, **5** and **6** with chemical shifts values (ppm). Pz 6* indicates the aggregated form of iron Pz.

The Mössbauer spectroscopy is a unique method, which allows for direct detection of all valence and spin states of heme-iron in Pz **6**. In Fig. 4, the Mössbauer spectrum of Pz **6**, measured at 85 K, is presented. Theoretical evaluation of the experimental data

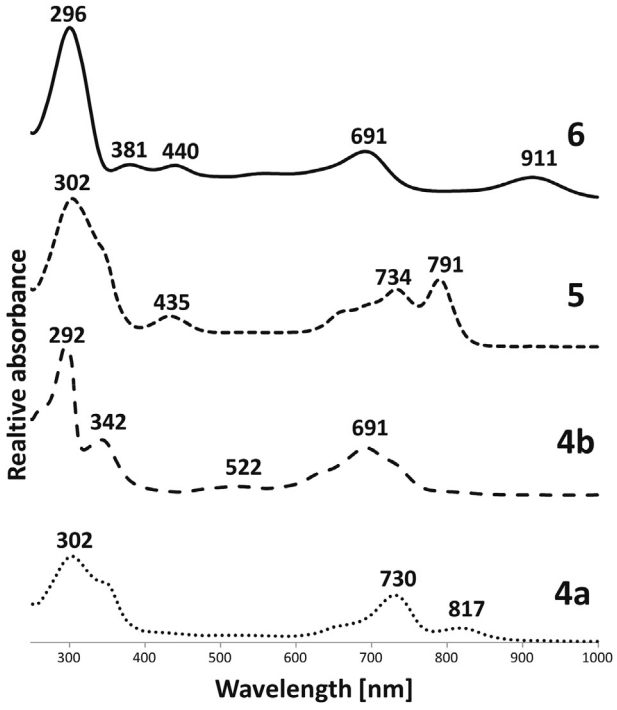

Fig. 3. Relative absorption spectra of **4a**, **4b**, **5** and **6** in CH_2Cl_2.

provides values of hyperfine parameters, an isomer shift (IS) and a quadrupole splitting (QS). They are very sensitive to the chemical character and arrangement of probing atom ligands (in our case ^{57}Fe) [31,32]. At least five subcomponents were necessary to get a good quality fit of the spectrum for Pz **6**. The line widths of about 0.18 ± 0.02 obtained for the subspectra indicate high homogeneity of the heme–iron binding sites. Heme-iron stabilized in a low spin ferrous state (in a diamagnetic state, Fe^{2+} with $S = 0$), characterized by IS = 0.18 ± 0.01 mm/s and QS = 0.24 ± 0.02 mm/s, has the highest contribution in the Mössbauer spectrum (about 35%). This state is formed in a case of strong covalent bonds between the iron atom and its ligands in a highly symmetric arrangement, for 6- or 4- coordinated iron [33]. Moreover, a component with IS = 0.12 ± 0.06 mm/s and QS = 2.88 ± 0.05 mm/s has a contribution of about 25.8 ± 3.0%. Such parameters are typical for iron in octahedral coordination, when one of the perpendicular ligands

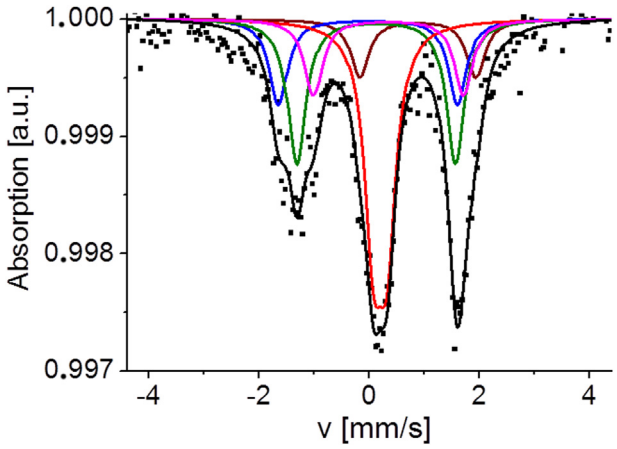

Fig. 4. The Mössbauer spectrum of Pz **6** at 85 K.

has a different chemical character than the others. It was very often observed for heme-iron, ligated with O_2, when the iron atom was in a low spin Fe^{2+} state [34]. A subspectrum, with IS of about 0.00 ± 0.10 mm/s and QS of about 3.28 ± 0.21 mm/s, is most probably also related to a diamagnetic state of heme-iron, but with a stronger distortion in its first coordination sphere. For example, a non-planar Pz ring may result in an additional increase of an electric field gradient. The contribution of this heme-iron state is about 15.3 ± 3.0%. In addition, a component with hyperfine parameters IS = 0.34 ± 0.06 mm/s and QS = 2.20 ± 0.10 mm/s can be ascribed to an intermediate spin state of Fe^{2+}. Such a state, which is formed when the d_{x2-y2} orbital has higher energy than the other orbitals, is typical for an intermediate spin state of reduced iron [35]. The Fe^{2+} state with $S = 1$ may originate from a tangled Pz ring. Its content in the Mössbauer spectrum is about 13.6 ± 3.0%. Notable, a high spin iron state is formed in Pz **6** (its contribution is about 10.3 ± 3.0%). A diamagnetic state of iron is rather present in Pz associates.

4. Conclusions

The expansion of peripheral pyrrolyl groups by 2,5-diphenyl substituents did not hamper the formation of the Pz associates in solution and solid-state. The interdigitation of the phenyl substituents, as observed in single crystal X-ray structure of magnesium(II) porphyrazine, led to Mg···Mg distance of ca. 11.2 Å in the dimer. The situation here was totally different from that reported for Pzs pairs with the associated centroid–centroid or metal ion – metal ion distances being ca. one half of that herein observed [5]. Moreover, 2,5-diphenylpyrrol-1-yl peripheral groups influenced the spin states of iron(II) Pz analog, which was confirmed by Mössbauer spectroscopy. Moreover, another bulky periphery present in tetraanthracenotetraazaporphyrins, researched by Fitzgerald et al. [28], prevented its iron analog from μ-oxo dimerization and resulted in its unexpected selectivity. In addition, the environment of heme-iron in Pz **6** is heterogenous that results in Fe^{2+} stabilization at various spin states. An extension of this work to the synthesis and Mössbauer spectroscopy studies of iron Pzs possessing different numbers of phenyl substituted pyrrolyl groups and their interactions, will be reported in due course.

Acknowledgments

This study was supported by the National Science Centre under Grant No. N N404 069440 and the European Fund for Regional Development No UDA-POIG.02.01.00-30-182/09. This work was performed within the BIONAN cooperation. T.G. thanks MSc Mariusz Duda for preliminary synthetic studies.

Appendix A. Supplementary data

Supplementary data related to this article can be found at http://dx.doi.org/10.1016/j.dyepig.2014.06.033.

References

[1] Trivedi ER, Harney AS, Olive MB, Podgorski I, Moin K, Sloane BF, et al. Chiral porphyrazine near-IR optical imaging agent exhibiting preferential tumor accumulation. Proc Natl Acad Sci U S A 2010;107:1284–8.
[2] Manet I, Manoli F, Donzello MP, Viola E, Masi A, Andreano G, et al. Pyrazinoporphyrazines with externally appended pyridine rings. 13. Structure, UV–Visible spectral features, and noncovalent interaction with DNA of a positively charged binuclear (Zn^{II}/Pt^{II}) macrocycle with multimodal anticancer potentialities. Inorg Chem 2013;52:321–8.
[3] Dubinina TV, Dyumaeva DV, Trashin SA, Sedova MV, Dudnik AS, Borisova NE, et al. Novel planar and sandwich-type complexes of substituted tetrathieno [2,3-b] porphyrazine: synthesis and investigation of properties. Dyes Pigm 2013;96:699–704.
[4] Rodriguez-Morgade MS, Stuzhin PA. The chemistry of porphyrazines: an overview. J Porphyrins Phthalocyanines 2004;8:1129–65.
[5] Michel SLJ, Hoffman BM, Baum SM, Barrett AGM. Peripherally functionalized porphyrazines: novel metallomacrocycles with broad, untapped potential. In: Karlin KD, editor. Progress in inorganic chemistry50. New York: J. Wiley & Sons; 2001. pp. 473–590.
[6] Liao MS, Watts JD, Huang MJ. FeII in different Macrocycles: electronic structures and properties. J Phys Chem 2005;109:7988–8000.
[7] Theodoridis A, Maigut J, Puchta R, Kudrik EV, van Eldik R. Novel Iron(III) porphyrazine complex. Complex speciation and reactions with no and H_2O_2. Inorg Chem 2008;47:2994–3013.
[8] Zhang Z, Peng Q, Sun J, Fang L, Deng K. Enhancement of catalytic activities of a biomimetic catalyst $FePz(dtnCl_2)_4$ for the wet oxidation of brilliant red X3B through the synergetic effect of heat and light irradiation. Ind Eng Chem Res 2013;52:13342–9.
[9] Donzello MP, Ercolani C, Stuzhin PA. Novel families of phthalocyanine-like macrocycles—Porphyrazines with annulated strongly electron-withdrawing 1,2,5-thia/selenodiazole rings. Coord Chem Rev 2006;250:1530–61.
[10] Goslinski T, Osmalek T, Mielcarek J. Photochemical and spectral characterization of peripherally modified porphyrazines. Polyhedron 2009;28:3839–43.
[11] Luo Q, Cheng S, Tian H. Synthesis and photochromism of a new binuclear porphyrazinato magnesium(II). Tetrahedron Lett 2004;45:7737–40.
[12] Goslinski T, Tykarska E, Szczolko W, Osmalek T, Smigielska A, Walorczyk S, et al. Synthesis and characterization of periphery-functionalized porphyrazines containing mixed pyrrolyl and pyridylmethylamino groups. J Porphyrins Phthalocyanines 2009;13:223–34.
[13] Szczolko W, Sobotta L, Fita P, Koczorowski T, Mikus M, Gdaniec M, et al. Synthesis, characteristics and photochemical studies of novel porphyrazines possessing peripheral 2,5-dimethylpyrrol-1-yl and dimethylamino groups. Tetrahedron Lett 2012;53:2040–4.
[14] Sobotta L, Fita P, Szczolko W, Wrotynski M, Wierzchowski M, Goslinski T, et al. Functional singlet oxygen generators based on porphyrazines with peripheral 2,5-dimethylpyrrol-1-yl and dimethylamino groups. J Photochem Photobiol A 2013;269:9–16.
[15] Goslinski T, White AJP. Synthesis, characterization and spectroscopic properties of novel periphery – functionalized unsymmetrical porphyrazines containing mixed dithienylpyrrolyl and dimethylamino groups. Polyhedron 2009;28:2579–84.
[16] Agilent Technologies. CrysAlis PRO software. Yarnton, Oxfordshire, England: Agilent Technologies; 2009.
[17] Burla MC, Caliandro R, Camalli M, Carrozzini B, Cascarano GL, De Caro L, et al. SIR2004: an improved tool for crystal structure determination and refinement. J Appl Cryst 2005;38:381–8.
[18] Sheldrick GM. A short history of SHELX. Acta Crystallogr 2008;A64:112–22.
[19] Rancourt DG, Ping JY. Voigt-based methods for arbitrary-shape static hyperfine parameter distributions in Mössbauer spectroscopy. Nucl Instrum Methods 1991;B58:85–97.
[20] Begland RW, Hartter DR, Jones FN, Sam DJ, Sheppard WA, Webster OW, et al. Hydrogen cyanide chemistry. VIII. New chemistry of diaminomaleonitrile. Heterocyclic synthesis. J Org Chem 1974;39:2341–50.
[21] Baum SM, Trabanco AA, Montalban AG, Micallef AS, Zhong C, Meunier HG, et al. Synthesis and reactions of aminoporphyrazines with annulated five- and seven-membered rings. J Org Chem 2003;68:1665–70.
[22] Linstead RP, Whalley M. 944. Conjugated macrocylces. Part XXII. Tetrazaporphin and its metallic derivatives. J Chem Soc 1952:4839–46.
[23] Decréau R, Chanon M, Julliard M. Synthesis and characterization of a series of hexadecachlorinated phthalocyanines. Inorg Chim Acta 1999;293:80–7.
[24] Zhong C, Zhao M, Goslinski T, Stern C, Barrett AGM, Hoffman BM. Porphyrazines peripherally functionalized with hybrid ligands as molecular scaffolds for bimetallic metal-ion coordination. Inorg Chem 2006;45:3983–9.
[25] Wierzchowski M, Sobotta L, Skupin-Mrugalska P, Kruk J, Jusiak W, Yee M, et al. Phthalocyanines functionalized with 2-methyl-5-nitro-1H-imidazolylethoxy and 1,4,7-trioxanonyl moieties and the effect of metronidazole substitution on photocytotoxicity. J Inorg Biochem 2013;127:62–72.
[26] Kameyama K, Morisue M, Satake A, Kobuke Y. Highly fluorescent self-coordinated phthalocyanine dimers. Angew Chem Int Ed 2005;44:4763–6.
[27] Niu L, Zhong C, Chen Z, Zhang Z, Li Z, Zhang F, et al. Novel azobenzene-phthalocyanine dyads—design of photo-modulated J-aggregation. Chin Sci Bull 2009;54:1169–75.
[28] Fitzgerald JP, Lebenson JR, Wang G, Yee GT, Noll BC, Sommer RD. Iron tetraanthracenotetraazaporphyrins: synthesis, structural characterization, ligand binding properties, and unexpected selectivity of a Bis-"Bowl" tetraazaporphyrin. Inorg Chem 2008;47:4520–30.
[29] Bauer EM, Cardarilli D, Ercolani C, Stuzhin PA, Russo U. Tetrakis(thiadiazole) porphyrazines. 2. Metal complexes with Mn(II), Fe(II), Co(II), Ni(II), and Zn(II). Inorg Chem 1999;38:6114–20.
[30] Adebayo AI, Nyokong T. Synthesis, spectroscopic and electrochemical properties of manganese, nickel and iron octakis-(2-diethylaminoethanethiol)-phthalocyanine. Polyhedron 2009;28:2831–8.
[31] Burda K, Hrynkiewicz A, Kołoczek H, Stanek J, Strzałka K. Molecular dynamics and local electronic states of Sn and Fe in metallocytochrome and metalloporphyrin. Hyp Int 1994;91:891–7.

[32] Burda K, Hrynkiewicz A, Kołoczek H, Stanek J, Strzałka K. Mixed valence state in ironporphyrin aggregates. Biochim Biophys Acta 1995;1244:345–50.
[33] Burda K, Kruk J, Borgstadt R, Stanek J, Strzałka K, Schmid GH, et al. Mössbauer studies of the non-heme iron and cytochrome b_{559} in a *Chlamydomonas reinhardtii* PSI– mutant and their interactions with α-tocopherol quinone. FEBS Lett 2003;535:159–65.
[34] Lang G, Marshall W. Mössbauer effect in some haemoglobin compounds. Proc Phys Soc 1966;87:3–34.
[35] Hu C, Noll BC, Schulz CE, Scheidt WR. Four-coordinate iron(II) porphyrinates: electronic configuration change by intermolecular interaction. Inorg Chem 2007;46:619–21.